Upgrading gasoline production through optimizing zeolite properties in the direct hydrogenation of CO_2/CO

Onintze Parra, Ander Portillo, Zuria Tabernilla, Andrés T. Aguayo, Javier Ereña, Javier Bilbao, Ainara Ateka *

Department of Chemical Engineering, University of the Basque Country UPV/EHU, P.O. Box 644, Bilbao, 48080, Spain

A R T I C L E   I N F O

A B S T R A C T

Role of HZSM-5 zeolite properties (in tandem with $ZnO–ZrO_2$) in direct synthesis of C_{5+} hydrocarbons from CO_2/CO was studied. The runs were performed in fixed bed reactor at: 420 °C; 50 bar; space time, 10 g_{cat} h mol_C^{-1}; H_2/CO_x, 3; CO_2/CO_x, 0.5. Two conventional zeolites were used (with SiO_2/Al_2O_3 ratio of 30 and 280), another one doped with Zn and one nano-sized zeolite with SiO_2/Al_2O_3 ratio of 371. It was determined that acidity conditions the performance of the catalyst, and the best results (yield and selectivity of C_{5+} of 19.6% and 78.0%, respectively, with a CO_x conversion of 25.1%) were obtained with nano-sized zeolite (low acidity). In the C_{5+} fraction, the major components were C_5 and C_6 paraffins, mostly isoparaffinic; so this fraction (without aromatics and with RON 91) is suitable for incorporating into gasoline pool. The presence of highly acidic sites favors secondary reactions of formation of C_1-C_4 hydrocarbons, by cracking and hydrogen transfer reactions, decreasing the CO_x conversion by worsening the synergy between the catalysts. Results are explained by the effect of the acidity on the extent of the stages of reaction network on $ZnO–ZrO_2$/HZSM-5 catalyst, and on synergy between the catalysts.

1. Introduction

The increase in carbon dioxide (CO_2) emissions associated with the consumption of fossil fuels, together with nitrogen oxide (N_2O) and methane (CH_4) emissions, have resulted in the development of phenomena such as climate change and ocean acidification, generating serious problems for humanity [1]. To reverse this situation and meet the growing demand for energy, high-income countries are promoting decarbonization strategies in their industrial activities and the progressive replacement of fossil fuels with renewables [2]. In this scenario, sustainable production of fuels and chemicals from CO_2 through carbon capture and utilization (CCU) technologies is receiving a great deal of attention in the transition period towards the general use of renewable energy [3].

CCU technologies are mainly catalytic processes using CO_2 as carbon source and oriented to the selective production of CO, methane, different oxygenates (methanol, dimethyl ether (DME), ethanol) [4] and hydrocarbons (olefins, BTEX aromatics, gasoline) [5]. For these processes is key the utilization of green H_2 [6]. In addition to the commercial interest in these products, which are in high demand, there is also the incentive to avoid CO_2 emission taxes. Among the CCU technologies, methanol synthesis is the most developed, using different catalysts [7] and especially made Cu-based [8]. The industrial process

is based on the background knowledge of the process using syngas (derived from carbon and natural gas) as feedstock. Therefore, the co-feeding of syngas together with CO_2 in CCU processes is interesting to provide a fraction of the required H_2.

The development of CCU technologies is demanding a high level of research activity in process intensification and in the *ad hoc* design of new catalysts. Thus, the direct production of hydrocarbons (fuels and chemicals) from CO_2 is studied by two alternative routes [9] both with tandem catalysts and integrating two reaction stages in the same reactor [10]. In the modified Fischer Tropsch (MFT) synthesis, a catalyst for FT synthesis (usually Fe- or Co-based) is combined with a selective acid zeotype, for the *in situ* production of hydrocarbons, adapting the composition of the products to the desired composition (with an Anderson–Schulz–Flory (ASF) distribution). The properties that affect the selectivity of the zeolite are the topology [11] and acidity [12]. In the route of synthesis of hydrocarbons with methanol as intermediate, the tandem catalyst (termed OX/ZEO (metallic oxide/zeotype)) is the combination of a methanol synthesis catalyst and a selective zeotype [13]. This route has as main attractions: (i) the non-existence of the ASF distribution restrictions; (ii) the thermodynamic advantage of shifting the equilibrium of the methanol synthesis step

---

* Corresponding author.
E-mail addresses: onintze.parra@ehu.eus (O. Parra), ainara.ateka@ehu.eus (A. Ateka).

by its *in situ* dehydration to DME [14], which is more reactive than methanol [15], and to hydrocarbons; (iii) the good knowledge of the reaction mechanisms of the methanol synthesis step from CO_2/CO (with formate ions as intermediates) [16] and of the effect of the nature of the active sites of this mechanism [17]. Likewise, it is well established the selective conversion of methanol/DME to light olefins, BTEX aromatics or gasoline (following the dual-cycle mechanism) over SAPO-34 and HZSM-5 catalysts [18]. However, the utilization of the information on these individual steps is conditioned by the different operating conditions and reaction medium in the integrated process. Thus, to achieve good synergy between the steps, the temperature and pressure need to be intermediate between the optimum for each step. Moreover, the different composition of the reactant streams has a remarkable incidence on the yield and product distribution, and on the deactivation of each catalysts in the tandem [19].

The metal catalysts used to configure the tandem catalysts in the direct synthesis of hydrocarbons from CO_2 have traditionally been Cu-based catalysts, since Cu–ZnO–Al$_2$O$_3$ has been the most commercially used in the synthesis of methanol from syngas [20] and also performs well in the synthesis from CO_2 [8,21], even using different preparation methods, such as uncalcined Cu-based catalysts [22]. However, partial sintering of Cu is inevitable at the temperature of the integrated process (above 300 °C to favor the conversion of methanol/DME into hydrocarbons) and also with a high concentration of H_2O (higher in CO_2 hydrogenation compared to CO), favoring Cu sintering. To avoid this problem, more hydrothermally stable metal oxides with different configurations have been used as catalysts, such as $ZnCr_2O_4$ [23], In_2O_3-ZrO_2 [24], $PdZn/ZrO_2$ [25], Ga_mCrO_x [26], ZnO–ZrO_2 [27] and ZrO_2-Cr [28]. These metallic oxides have been combined with different zeotypes, such as SAPO-34 for the selective production of olefins (with In_2O_3/SAPO-34 [29], ZnZrO/SAPO-34 [30] and Ga_mCrO_x [26]) or light paraffins (with $PdZn/ZrO_2$ [25]). The combination with HZSM-5 zeolite has been used for the selective production of BTEX aromatics (with $ZnCr_2O_4$/HZSM-5 [23] and ZrO_2-Cr/HZSM-5@SiO_2 [28]) or hydrocarbons in the range of gasoline (with ZnO–ZrO_2/HZSM-5 [31]). Ghosh et al. [32] propose a kinetic model for this hydrocarbon production process. It should be noted that the aforementioned works correspond mostly to CO_2 conversion and that studies of direct synthesis of hydrocarbons co-feeding syngas together with CO_2 are limited, and oriented to the production of olefins [29] and gasoline [33].

The stability and selectivity of the ZnO–ZrO_2 oxides in the CO_2 hydrogenation to methanol is highlighted in the literature [34] and it is a consequence of the formation of a $ZnZrO_x$ solid solution, with the Zn incorporated into the ZrO_2 lattice matrix [35]. Ticali et al. [36] obtained olefins or paraffins with the $ZnZrO_2$ catalyst combined with SAPO-34 and HZSM-5, respectively. These authors explain the selective production of paraffins with the $ZnZrO_x$/HZSM-5 catalyst from CO_2 hydrogenation, rather than the production of aromatics obtained by other authors with this combination of catalysts (with nano-sized zeolite [37] and with hierarchical pore structure [38]), highlighting the importance of different factors as the composition of the $ZnZrO_x$ catalyst, the acidity of the zeolite, the OX/ZEO ratio, and the reaction conditions.

The use of the HZSM-5 zeolite in the OX/ZEO tandem catalyst is especially interesting for the selective production of gasoline. This way, it was originally proposed for the selective production of gasoline from methanol (MTG process) [39] and its selectivity and limited deactivation by coke are explained by its moderate acidity and shape selectivity characteristics of its MFI structure, with two intersected channels (sinusoidal of 0.51 *x* 0.55 nm and straight of 0.53 *x* 0.56 mm), and no cages at the intersections [40]. It is also remarkable the ability to improve the selectivity and stability of the HZSM-5 zeolite in the conversion of methanol into hydrocarbons through different initiatives. Thus, increasing the SiO_2/Al_2O_3 ratio decreases the density of Brønsted acid sites, which favors the formation of olefins. In addition, it increases the propylene/ethylene ratio (by favoring the olefins cycle with respect

to the aromatics cycle [41]) and disfavors secondary reactions [42] and coke formation, as demonstrated in the conversion of DME to olefins [43] and methanol to hydrocarbons [44]. The decrease in zeolite crystal size is effective for minimizing the extent of secondary reactions [45] (dealkylation, cracking, hydrogen transfer), favoring the selective formation of olefins as primary products [46] and minimizing the diffusional limitations of coke precursors [47]. Metal incorporation is also extensively used to modulate zeolite acidity and pore volume distribution, with the intention of increasing stability and improving product distribution. Wen et al. [48] decreased the acidic strength of HZSM-5 zeolite with the incorporation of Ni, which also favors the selective formation of isoparaffins from DME. However, as previously mentioned, reaction conditions have also a strong impact on the extent of the reaction and deactivation mechanisms in the direct conversion of CO_2 into hydrocarbons. Thus, based on the results for the conversion of methanol [49] and DME [43] to hydrocarbons, the high partial pressure of H_2, the presence of steam and an active catalyst for the hydrogenation of coke precursors may contribute to limit the deactivation of zeolite by coke. This moderate deactivation has been found even at high pressure and with high concentration of aromatics (active condensed-coke precursors) [50].

Nonetheless, Vosmerikova et al. [51] highlight the stability and high selectivity of isoparaffins using a Zn-isomorphously substituted HZSM-5 catalyst under conditions typical of DME synthesis (50–100 bar and 300–340 °C) and co-feeding H_2, CO and CO_2 as corresponds to the DME synthesis stream from syngas. This performance is explained by the hydroisomerization activity of Zn, due to its proven ability to facilitate the H_2 dissociation, as demonstrated in the conversion of DME in hydrocarbons [51] and in the selective production of isoparaffinic gasoline [52].

In view of these antecedents, in this work the performance of a ZnO–ZrO_2/HZSM-5 tandem catalyst in the selective production of C_{5+} hydrocarbons (with an isoparaffinic composition, of interest for their incorporation into the gasoline pool) was studied. Attention was focused on the properties (especially acidity) of the HZSM-5 zeolite catalyst, using HZSM-5 zeolites with different configuration: conventional (microsized crystals) with different SiO_2/Al_2O_3 ratio, with nano-sized crystals, and doped with Zn. The effect of zeolite properties on the selectivity and composition of gasoline is explained with the reaction network of the integrated process, considering the role of the properties in the extent of the individual reaction steps and in the synergy between the steps of synthesis of oxygenates and their conversion into hydrocarbons. The application of the criteria established for the conversion of methanol to hydrocarbons over HZSM-5 zeolite, considering the crystal size [53] and Al content [54], facilitates the explanation of the distribution of products in the particular conditions of the integrated process.

2. Material and methods

2.1. Preparation of the catalysts

The catalyst for the methanol synthesis step, ZnO–ZrO_2 (named ZZ in a simplified way), was synthesized with an atomic Zn/Zr ratio of 1/2.5 by a co-precipitation method described in a previous work [31]. This catalyst was selected because of its good performance in the tandem catalyst for the one stage conversion of CO_2/CO mixtures into gasoline-range hydrocarbons [31].

Regarding the acid catalysts, they are based on HZSM-5 with different properties, as described as follows with reference to its simplified designation: the named nH371 is a nanozeolite (ACS Materials, MSZ5N522), with a SiO_2/Al_2O_3 molar ratio of 371. H30 and H280 are two microporous zeolites (Zeolyst International, CBV-3024E and CBV-28014), with a SiO_2/Al_2O_3 molar ratio of 30 and 280, respectively. ZnH30 is a Zn-modified microporous HZSM-5 zeolite with SiO_2/Al_2O_3 molar ratio of 30, which was prepared by ion exchange [55], placing

the precursor nitrate solution $(Zn(NO_3)_2 \cdot 6H_2O)$ in contact with the zeolite powder in a flask, under continuous stirring at 60 °C for 24 h. The doped zeolite powder (with 2% Zn) was agglomerated by wet extrusion in a matrix (50 wt%), using a colloidal dispersion of α-alumina (Alfa-Aesar, 18 wt%) and pseudoboehmite (Sasol Germany, 32 wt%). All the original zeolites were provided in ammonium form and, consequently, calcined at 575 °C for 2 h to obtain the acid form. This calcination stage causes the conversion of the pseudoboehmite in the ZnH30 catalyst into γ-Al_2O_3 [56].

The tandem catalysts (ZZ/nH371, ZZ/H280, ZZ/ZnH30 and ZZ/H30) were prepared by physical mixture of the metallic oxide and the zeolites, with a particle size in the 125–250 and 300–400 μm range, respectively, with a ZZ/zeolite mass ratio of 1/1.

2.2. Characterization of the acid catalysts

The structural properties were determined by X-ray diffraction (XRD) by means of a PANalyitical Xpert PRO diffractometer. The measurement conditions were 40 kV/40 mA, and the pattern was recorded in a 5°< 2θ < 80° range. The textural properties (specific surface area, pore- and micropore volume) were measured by N_2 adsorption–desorption isotherms at −196 °C (Micromeritics ASAP 2010). For this analysis, prior to the test, the sample was degassed for 8 h under vacuum conditions to ensure the elimination of H_2O and impurities adsorbed on the sample. Afterwards, sequential equilibrium stages of N_2 adsorption–desorption were performed until the complete saturation of the sample. The specific surface area (S_{BET}) was calculated using the Brunauer–Emmett–Teller (BET) equation, the pore volume was determined using the Barrett–Joyner–Halenda (BJH) method and the micropore volume and surface were obtained by means of the t-plot method.

The acidity of the catalysts was determined by temperature programmed desorption of NH_3 (TPD-NH_3) (Micromeritics Autochem 2920). Initially, the sample was swept with He (160 cm^3 min^{-1}) at 550 °C for 30 min, in order to eliminate impurities and H_2O, and stabilized at 150 °C with He (20 cm^3 min^{-1}). Subsequently, 5 cm^3 min^{-1} NH_3 injections were conducted until the saturation of the sample and then swept with He (50 cm^3 min^{-1}) to remove the physically adsorbed NH_3. Lastly, the NH_3 desorption was carried out by heating the sample up to 550 °C, following a 5 °C min^{-1} heating rate.

The nature of the acid sites of the catalysts, Brønsted or Lewis (BAS and LAS, respectively), was determined by FTIR (Fourier transform infrared spectroscopy) of adsorbed pyridine (Py-FTIR) in a Nicolet 6700 spectrophotometer (Thermo-Fisher Scientific) coupled to a Specac high-temperature high-pressure (HTHP) cell. The vibrational bands assigned to each type of acid sites are well known in the literature [57, 58]: 1545 cm^{-1} for Brønsted-type sites (molar extinction coefficient of 1.67 cm μmol^{-1}) and 1445 cm^{-1} for Lewis-type sites (molar extinction coefficient of 2.22 cm μmol^{-1}).

2.3. Reaction and analysis equipment

The hydrogenation reactions were carried out in a reaction equipment (PID Eng. & Tech. Microactivity Reference), outlined in detail in Figure S1. The catalyst packed bed consists of a mixture of the catalyst diluted in SiC inert solid, in order to ensure bed temperature uniformity, to avoid preferential paths and to ascertain a suitable bed height when operating al low space time values. The feed and the products stream were analyzed on-line in a micro chromatograph (Varian CP-4900, Agilent), equipped with three chromatographic columns: (i) molecular sieve (MS-5) (10 m x 12 μm) to identify and quantify H_2, O_2, N_2 and CO; (ii) Porapak Q (10 m x 20 μm) to identify and quantify CO_2, methane, H_2O, C_2-C_4 hydrocarbons, methanol and DME; and (iii) 5 CB (CPSiL) (8 m x 2 μm) to identify and quantify C_{5+} hydrocarbons. The columns are periodically calibrated with standard mixtures.

The reaction runs were conducted under the following conditions, established previously as optimal [31]: 420 °C; 50 bar; space time, 10 g_{cat} h mol_C^{-1}; CO_2/CO_x molar ratio in the feed, 0.5; H_2/CO_x molar ratio in the feed, 3. The catalyst was subjected to a partial reduction prior to the reaction in a diluted H_2 stream (30 cm^3 H_2 min^{-1} and 30 cm^3 N_2 min^{-1}) for 1 h at 350 °C and 2 bar.

2.4. Reaction indices

The results were quantified in terms of conversion of CO_x (CO_2 + CO), product yield and selectivity. The conversion of CO_x was defined as:

$$X_{CO_x} = \frac{F^0_{CO_x} - F_{CO_x}}{F^0_{CO_x}} \cdot 100 \tag{1}$$

where $F^0_{CO_x}$ and F_{CO_x} are the CO_x (CO_2+CO) molar flow rates at the inlet and outlet of the reactor, respectively.

Yield (Y_i) and selectivity (S_i) of each i carbonated product were calculated according to the following expressions:

$$Y_i = \frac{n_i \cdot F_i}{F^0_{CO_x}} \cdot 100 \tag{2}$$

$$S_i = \frac{n_i \cdot F_i}{\sum_i (n_i \cdot F_i)} \cdot 100 \tag{3}$$

where n_i is the number of carbon atoms in a molecule of i product, and F_i the molar rate of the i product in the product stream. All the molar flows in Eqs. (1)–(3) were quantified in content C atoms.

3. Results and discussion

3.1. Catalysts properties

The metallic ZZ catalyst was thoroughly characterized in a previous work [31]. The most relevant properties (textural properties and chemical composition) are gathered in Table S1 and Figure S2, respectively. The results of the textural properties of the acid catalysts are listed in Fig. 1 and Table 1. For a more detailed analysis of the isotherms, these are shown independently in Figure S3. All the catalysts, except for ZnH30, show a typical isotherm for microporous HZSM-5 zeolite, where N_2 is adsorbed in the low relative pressure region ($p/p_0 < 0.01$) [59]. In the case of ZnH30, N_2 is adsorbed at higher relative pressure due to the agglomeration with the matrix (formed by γ-Al_2O_3 and α-Al_2O_3), which confirms that a hierarchical porous structure is conferred [56]. Additionally, the incorporation of the metal contributes to reduce the S_{BET} from 391 m^2 g^{-1} for H30 to 253 m^2 g^{-1} for ZnH30. Comparing H30 and H280 zeolites it is observed that increasing SiO_2/Al_2O_3 ratio of HZSM-5 zeolites diminishes the S_{BET} and micropore volume. The smaller crystal size of the nH371 zeolite explains the slightly higher S_{BET} and micropore volume than that of H280 [60].

Table 1
Textural properties of the catalysts.

Catalyst	Surface area (m^2 g^{-1})		Pore volume (m^3 g^{-1})	
	BET	Micropore	Pore	Micropore
H30	391	292	0.218	0.126
ZnH30	253	107	0.260	0.050
H280	414	232	0.218	0.096
nH371	423	283	0.219	0.120

The NH_3-TPD profiles are depicted in Fig. 2, and the total acidity, temperature of the desorption peaks and the BAS/LAS ratio are summarized in Table 2. The zeolites can be ranked based on their total acidity in the following order: nH371 < H280 ≪ ZnH30 < H30. It should be noted that the value of the total acidity of ZnH30 considers the incorporation of the matrix, which reduces the acidity value of
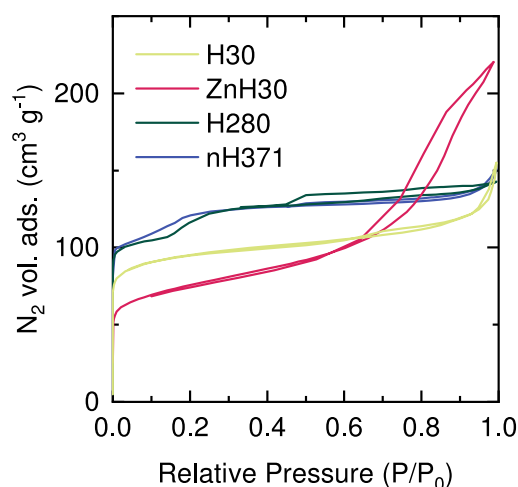
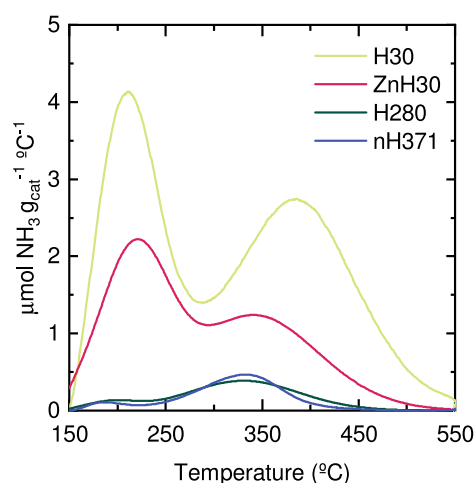**Fig. 1.** N$_2$ adsorption–desorption isotherms of the catalysts.

Fig. 2. NH$_3$-TPD profiles of the acid catalysts.

Table 2
Total acidity of the catalysts, temperature of the desorption peaks and BAS/LAS ratio.

Catalyst	Total acidity ($\mu mol_{NH_3} g_{cat}^{-1}$)	First peak (°C)	Second peak (°C)	BAS/LAS ratio
H30	759.8	212	383	4.30
ZnH30	376.5	220	342	1.10
H280	62.8	196	331	2.31
nH371	56.1	185	334	1.08

the zeolite by half. In all the NH$_3$-TPD profiles, two distinct peaks are observed, which help to classify acidity according to literature [61]: one at low desorption temperature, corresponding to weak acid sites; and, another peak at higher desorption temperature, corresponding to strong acid sites. It is noteworthy that, as established in literature [59], as SiO$_2$/Al$_2$O$_3$ ratio increases, a shift to lower desorption temperature and a lower intensity of the peaks is observed, which indicates that the acid strength is consequence of the Al^{3+} content [62].

The Py-FTIR spectra obtained for all acid catalysts are depicted in Fig. 3. As observed in Table 2, when increasing the SiO$_2$/Al$_2$O$_3$ ratio of the zeolite from 30 to 280, BAS/LAS ratio diminishes drastically from 4.30 to 2.31. Zn doping has an even higher incidence, decreasing the ratio to 1.10. This value is similar to that of the nH371 zeolite (1.08), corresponding to the majority proportion of weakly acidic sites.

Fig. 4 gathers the normalized XRD patterns of the catalysts. The pattern of the different HZSM-5 zeolites are almost identical, and they
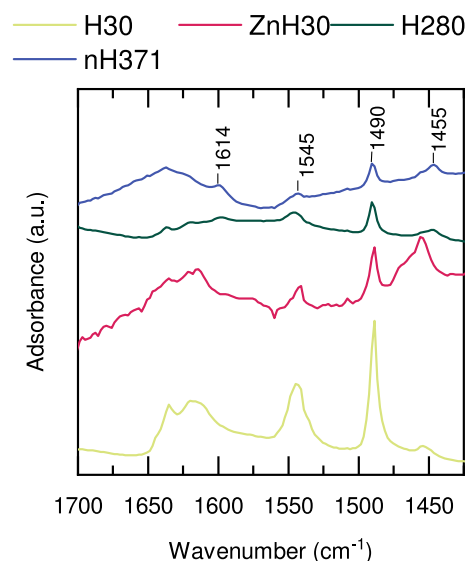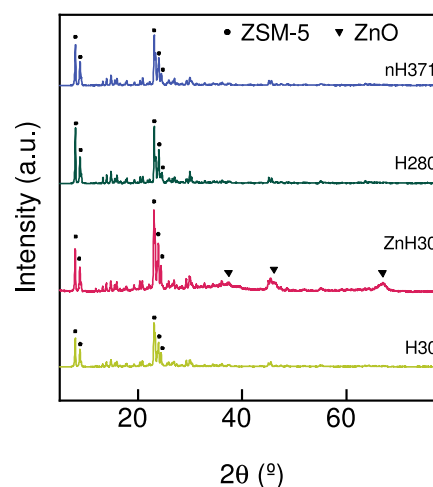

Fig. 3. Py-FTIR spectra of the acid catalysts.

Fig. 4. XRD patterns of the acid catalysts.

show two intense peaks at $2\theta \approx 7.9°$ and $2\theta \approx 8.8°$, and three other peaks at $2\theta \approx 23.1°$, $2\theta \approx 23.3°$ and $2\theta \approx 23.7°$. This diffractograms correspond to ZSM-5, in accordance with ICDD (International Center for Diffractional Data) #79-1638. As for ZnH30 catalyst, in addition to ZSM-5, peaks related to ZnO are observed at $2\theta \approx 36.3°$, $2\theta \approx 47.5°$ and $2\theta \approx 68.0°$ (in accordance with ICDD #36-1451).

Fig. 5 shows the SEM images of the acid catalysts. In Fig. 5(a), flake shaped agglomerates are observed for H30. These agglomerates are larger in ZnH30 catalyst (Fig. 5(b)). In Fig. 5(c), H280 shows irregular crystal shape, significantly larger than nH371, for which a polyhedral shape is observed (Fig. 5(d)).

3.2. Performance of the catalysts

3.2.1. Yield and selectivity

In this section, the performance of the different acid catalysts, in tandem with ZZ catalyst, was compared under the direct hydrogenation of CO$_2$/CO to hydrocarbons process conditions, with the aim of producing gasoline-range C$_{5+}$ hydrocarbons. In 6-hour runs on stream, it was proven that catalyst deactivation with ZZ/H280 and ZZ/nH371 was insignificant, with constant values of conversion and distribution
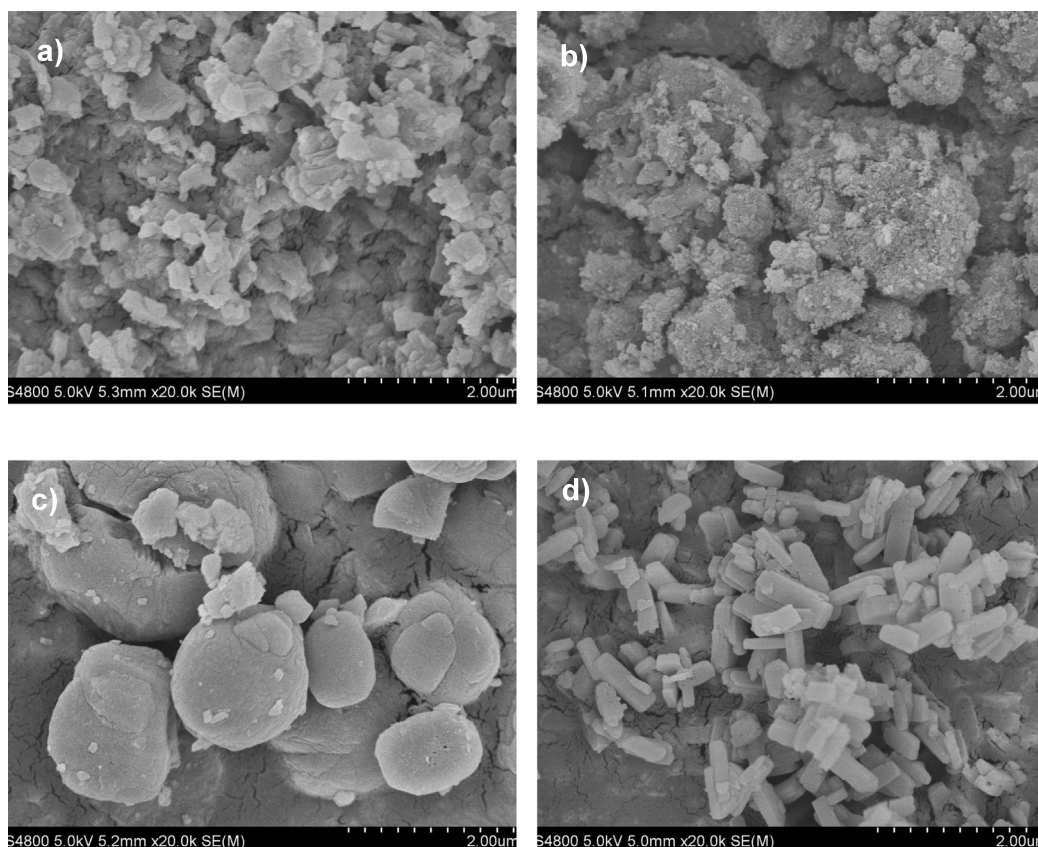
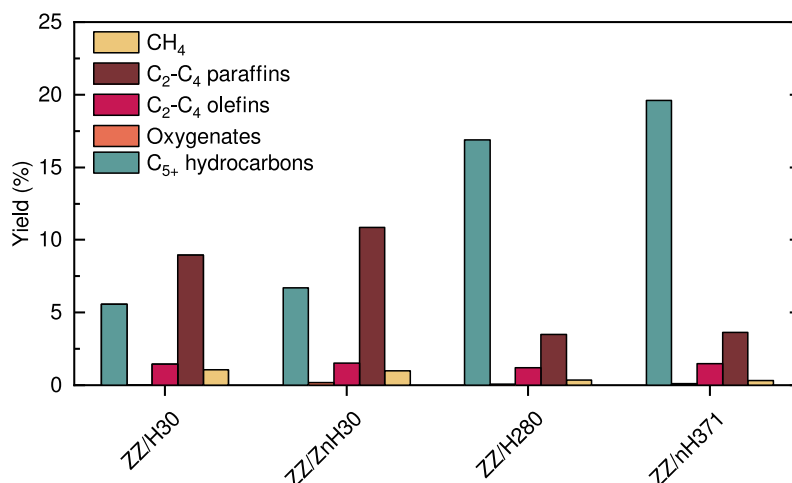**Fig. 5.** SEM images of (a) H30, (b) ZnH30, (c) H280 and (d) nH371.

Fig. 6. Comparison of products yield with different tandem catalysts. Reaction conditions: 420 °C, 50 bar, 10 g_{cat} h mol_C^{-1}, H_2/CO_x = 3, CO_2/CO_x = 0.5.

of products (Figure S4). Considering the slight deactivation of the other two catalysts (ZZ/H30 and ZZ/ZnH30), in order to ensure consistency of the results of this section, the results compared correspond to extrapolation at zero time on stream. Figs. 6 and 7 exhibit, respectively, the yield and selectivity of the significant product lumps, including CH_4, C_2-C_4 paraffins, C_2-C_4 olefins, oxygenates (methanol and DME) and C_{5+} hydrocarbons, and the CO_x conversion.

Regarding the performance of ZnH30 and H30 zeolites, the results obtained were similar, although slightly better yields were achieved with the addition of Zn in ZnH30. The yield of C_2-C_4 and C_{5+} hydrocarbons was nearly the same with both zeolites, reaching values of 8.9% and 5.6%, respectively, for ZZ/H30, and 10.9% and 6.7%,

respectively, for ZZ/ZnH30. The improvement in the conversion of the oxygenates (slight in this case) is attributed in the MTG process by Fattahi et al. [63] to the synergistic effect between the Zn and the acid sites of the zeolite. Additionally, the incorporation of Zn resulted in a slight increase of C_{5+} selectivity from 32.7% to 33.1% (Fig. 7). It is noteworthy that the oxygenate yield with all the zeolites was insignificant, accounting for less than 0.2% in all cases. This feature is indicative of practically complete conversion of oxygenates to hydrocarbons, and evidences the excellent synergy, under these reaction conditions, between the metallic oxide and the zeolite in the tandem catalyst. In terms of CO_x conversion, there was also an increase (from 17% to 20%) when adding Zn to the zeolite, which is in line with results
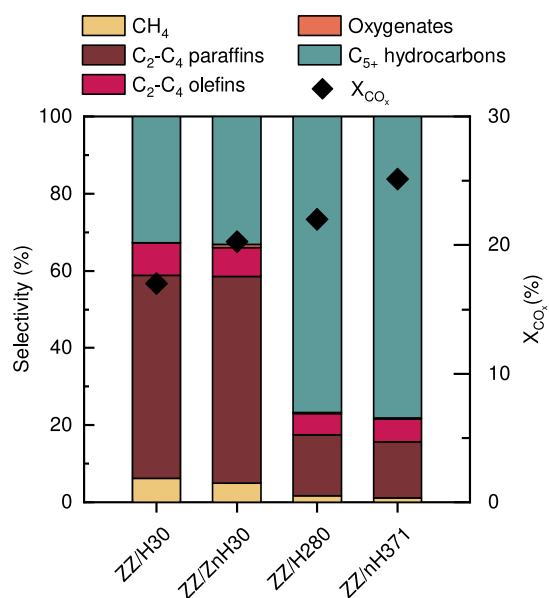
Fig. 7. Comparison of obtained products selectivity and CO_x conversion with different tandem catalysts. Reaction conditions: 420 °C, 50 bar, 10 g_{cat} h mol_C^{-1}, H_2/CO_x = 3, CO_2/CO_x = 0.5.

Fig. 8. Effect of zeolite acidity over products selectivity. Reaction conditions: 420 °C, 50 bar, 10 g_{cat} h mol_C^{-1}, H_2/CO_x = 3, CO_2/CO_x = 0.5.

in MTG [51] and MTA [64] processes. Jin et al. [65] emphasize the effect of the CO_2 content on these results.

Among HZSM-5 zeolites without metal incorporation, the SiO_2/Al_2O_3 ratio is one of the most important criteria for zeolite selection. The results obtained (Figs. 6 and 7) with zeolites with higher SiO_2/Al_2O_3 ratio (Table 2), such as nH371 and H280, were more interesting that those with a SiO_2/Al_2O_3 ratio of 30 (H30 zeolite) for the production of gasoline-range hydrocarbons (C_{5+} hydrocarbons), suggesting that the total acidity (that diminishes with increasing SiO_2/Al_2O_3 ratio, Table 2) plays a crucial role in product distribution. Thus, as well established in the MTG [42] and MTA processes [66], the secondary reactions of cracking are favored with a low SiO_2/Al_2O_3 ratio. As a consequence of these reactions, a notable yield and selectivity of C_2-C_4 paraffins and of CH_4 were obtained with both ZnH30 and H30 zeolites. It can be also observed that catalyst with nH371 zeolite exhibited the superior C_{5+} hydrocarbon yield, with a C_{5+} hydrocarbon yield of 19.6%. C_2-C_4 paraffins accounted for nearly 3.6%, and the yield of olefins and CH_4 was less than 2%. Similar findings were observed for C_2-C_4 paraffins and for CH_4 with H280 zeolite, with a C_{5+} yield slightly lower (16.9%) to that obtained with nH371 zeolite.

As to the selectivity and CO_x conversion regards (Fig. 7), as mentioned above with yields, the incorporation of Zn in the zeolite did not reveal a significant incidence. It is observed that the catalysts with higher SiO_2/Al_2O_3 ratio zeolites (nH371 and H280) exhibited higher CO_x conversion (25.1% and 22%, respectively) and C_{5+} selectivity (78% and 76.7%, respectively), with lower selectivity values of C_2-C_4 paraffins (14% for nH371 zeolite) and CH_4 (1.2% for these zeolites). It is worth noting that, in all cases, olefin selectivity remained below 10%. This is attributed to the high partial pressure of H_2 in the reaction medium and the presence of the ZZ metallic oxide, which exhibits a significant hydrogenating capability in these conditions, leading to the hydrogenation of olefins into paraffins [19].

The aforementioned results show the interest of using a HZSM-5 zeolite with a high SiO_2/Al_2O_3 ratio to favor the formation of hydrocarbons in the range of the gasoline. However, nH371 zeolite stands out as the most suitable candidate.

3.2.2. Role of the properties of the zeolite

The results in the previous section are consequence of the differences in the physical properties (Table 1) and acidity (Table 2) of the
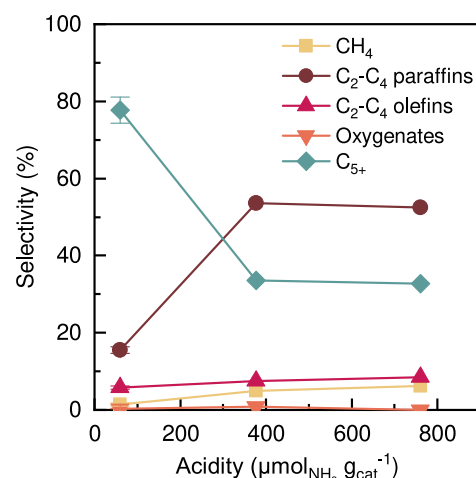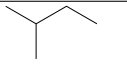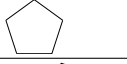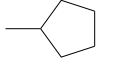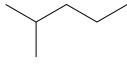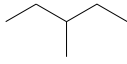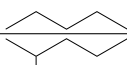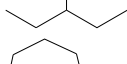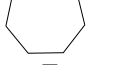
HZSM-5 zeolites utilized in the configuration of the tandem catalyst. Considering the relevance of the catalyst acidity in the methanol/DME conversion into hydrocarbons [67], in Fig. 8, the effect of this property of the HZSM-5 zeolites used in tandem catalysts was studied in selectivity terms. A clear trend between acidity and product distribution was observed, particularly for C_2-C_4 paraffins and C_{5+} hydrocarbons. This way, with zeolites with low acidity (< 100 $\mu mol_{NH_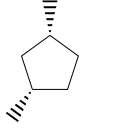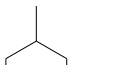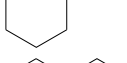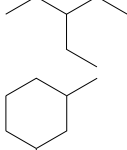3} g_{cat}^{-1}$, nH371 and H280 zeolites, with similar results), C_{5+} hydrocarbons prevailed. This selectivity decreased with increasing acidity, and highly acidic zeolites (> 400 $\mu mol_{NH_3} \cdot g_{cat}^{-1}$, ZnH30 and H30 zeolites) showed a 60% decrease in the selectivity of C_{5+} hydrocarbons and an increase in the selectivity of C_2-C_4 paraffins. These findings are explained in the conversion of methanol under MTG process conditions by the promotion of the cracking reactions by means of the strong acid sites in the zeolites, with the formation of C_2-C_4 olefins, C_2-C_4 paraffins and CH_4 [42,68]. Thus, the limited selectivity of C_2-C_4 olefins in Fig. 8 is a consequence of the hydrogenation to the corresponding paraffins.

It should be noted that the nH371 and H280 zeolites also have the lowest density of acid sites (taking into account the values of total acidity (Table 2) and BET surface area (Table 1)), minimizing the extent of undesired side reactions. These findings highlight the importance of the acidity of HZSM-5 also in the reaction conditions of this process (remarkably different from those of the MTG process) and suggest that zeolites with lower acidity are more suitable for producing gasoline-range hydrocarbons (C_{5+}).

The higher CO_x conversion with low acidity catalysts is not consistent with the expected effect of acidity, whose increase was expected to favor the displacement of the oxygenate (methanol/DME) formation equilibrium as a consequence of the higher extent of the conversion of the latter into primary hydrocarbons (olefins). The possible cause of these results is the relevance of the acidity in the contact-induced ion exchange phenomena observed in bifunctional catalysts. Thus, in the direct synthesis of DME from CO_2 over hybrid catalysts formed by CuO-ZnO-ZrO_2 and zeolites of different acidity, Bonura et al. [69] justify the higher reaction rate for an intermediate acid site density by the lower stability of the zeolite surface with increasing acidity, facilitating the migration of Cu^{2+} and Zn^{2+} ions by ion exchange with the zeolite protons. García-Trenco et al. [70] verified this negative effect of the interaction between metal oxides (Cu–ZnO–Al_2O_3) and the HZSM-5 zeolite of hybrids catalysts used in the synthesis of DME from syngas, emphasizing that the migration of ions is favored by the proximity of the acid and metallic active sites, by the presence of H_2O and the acidity of the zeolite [71]. Although the stability of the tandem catalyst prepared in this work by physical mixing of the metal

Table 3
Main C_{5+} compounds obtained with ZZ/nH371 catalyst.

Carbon number	Main compounds
C_5	2-Methylbutane
	n-Pentane
	Cyclopentane
C_6	Methylcyclopentane
	2-Methylpentane
	3-Methylpentane
	n-Hexane
C_{7+}	2-Methylhexane
	3-Methylhexane
	Cycloheptane
	Cis-1,3-Dimethylcyclopentane
	Methylcyclohexane
	Ethylpentane
	1,3-Dimethylcyclohexane

oxide catalyst and the zeolite is higher, the high reaction temperature (420 °C, much higher than the 260 °C of the DME synthesis) will favor this phenomenon of ion migration, justifying the convenience of using a zeolite with reduced density of acid sites. Redekop et al. [72] studied recently with different *ex situ* and *in situ* characterization techniques the structure of the ZnO–ZrO$_2$ catalyst used in methanol synthesis, verifying the mobility of Zn^{2+} species in the solid solution phase with ZnO, a phenomenon that is favored by the increase of temperature and that is reversible, recovering the original structure after the regeneration of the catalyst in oxidizing atmosphere. This result suggests the hypothesis that the proximity of Brønsted sites favors this reversible migration of Zn^{2+} species by decreasing the capacity of the ZnO–ZrO$_2$ catalyst in the integrated process.

Though the results in Fig. 8 highlight the role of acidity in product distribution, the role of zeolite porous structure in contributing to differences in product distribution results must also be considered. In addition to the higher SiO$_2$/Al$_2$O$_3$ ratio of the nH371 (and consequent lower acidity), the higher selectivity of C_{5+} hydrocarbons with this catalyst (Fig. 7) is in accordance with its nano-sized crystal (57 nm), which provides a larger surface area to the zeolite (Table 1). These properties favor the access of reactants and the diffusion of the products, and consequently, the extent of the oligomerization reactions of olefins, with formation of hydrocarbons of higher molecular weight [73]. On

the other hand, the slightly worse performance of ZnH30 with respect to H30 (in terms of C_{5+} selectivity, Fig. 7) is also in line with the lower surface area and micropore volume, facilitating the retention and cracking of hydrocarbons.

3.2.3. Product composition

Fig. 9 presents the product distribution in selectivity terms categorized by groups (n-paraffin, isoparaffin, olefin, and naphthene) and by carbon number for ZZ/H30, ZZ/H280 and ZZ/nH371 catalysts. Overall, ZZ/H280 (Fig. 9(b)) and ZZ/nH371 (Fig. 9(c)) exhibited similar results, with minor discrepancies in C_5 and C_6 isoparaffins and heavy naphthenes. In both cases, C_5 and C_6 branched-chain paraffins were the predominant product, with ZZ/nH371 yielding slightly better results, reporting a selectivity of 28.8% and 31.3% for C_5 and C_6, respectively. This is consistent with the literature's reported isomerization capacity of HZSM-5 [48,51,52]. It should be noted that 2-methylbutane, 2-methylpentane, and 3-methylpentane were the prominent isoparaffins in C_5 and C_6 category. ZZ/nH371 and ZZ/H280 catalysts exhibited low levels of n-paraffins, which were mostly present as methane, ethane, and propane, with their presence becoming less noticeable at higher carbon numbers. With ZZ/H30 catalyst (Fig. 9(a)), the product distribution is less interesting for the goal of gasoline production. C_4 and C_5 hydrocarbons were predominant, mainly isoparaffins, being noticeable the selectivity of lighter n-paraffins (with a selectivity exceeding 30% and with propane as majority). This trend can be attributed to the promotion of the cracking reactions by highly acid zeolites, as previously mentioned, and it is well established in the MTG process [42]. It is worth noting that the presence of olefins was minimal for all catalysts, owing to the high hydrogen pressure in the reaction. In fact, only C_4 olefins reached a selectivity of 7% with ZZ/H30 catalyst (Fig. 9(a)). This insignificant olefin content in the C_{5+} lump and the low aromatic content (selectivity below 0.1% and not depicted in Fig. 9) are beneficial for the incorporation of this lump into the gasoline pool in the refineries. This observation aligns with the previous finding of Vosmerikova et al. [51], who revealed that isomerization and aromatization reactions are competitive in the dual-cycle mechanism of methanol/DME conversion into hydrocarbons in the MTG process [74]. The activity of the HZSM-5 zeolite in paraffin isomerization is well established in literature [75], and it is favored with the accessibility of the external acid sites by the decrease of the crystal size [73]. Therefore, increasing the selectivity towards isoparaffins (due to the partial pressure of H_2 and the isomerizing activity of HZSM-5 zeolite under these conditions) attenuates the extent of dehydrocyclization reactions, leading to a decreased aromatic selectivity.

Table 3 shows the itemization of the main C_{5+} hydrocarbons obtained with ZZ/nH371 zeolite. In the five carbon atom group, isoparaffins were predominant, whereas also linear and naphthene compounds were also detected. By increasing the number of carbons, branched paraffins (2-methylpentane and 3-methylpentane) predominate, with a very low presence of n-hexane and naphthenes. Hydrocarbons with more than 7 carbon atoms comprised isoparaffins and naphthenes, with negligible presence of linear paraffins, olefins and aromatics. The high presence of isoparaffinic hydrocarbons leads to a high Research Octane Number (RON) of the hydrocarbon product obtained, which exceeded 91, calculated according to the method proposed by Anderson, Sharkey and Walsh [76], from the composition.

3.2.4. Discussion

The effect of the properties of the HZSM-5 in the tandem catalyst on the conversion of CO_x, yield and distribution of hydrocarbons has been explained in the previous sections mainly using the knowledge in the literature of the conversion of methanol to hydrocarbons. This reaction that is performed under different conditions than those of the integrated process studied in this work. In this section, the results are justified considering the conditions of the integrated process, and the role of the synergy between its two main stages. In addition, the
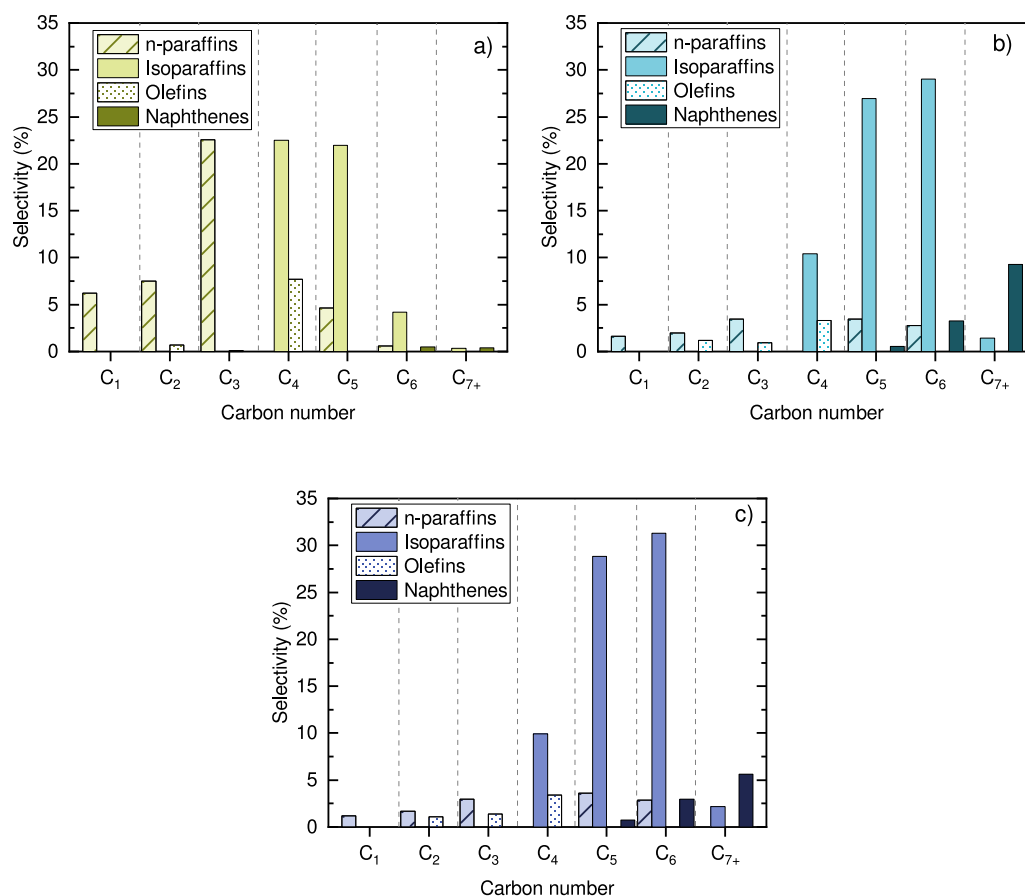
Fig. 9. Product distribution, classified by carbon number for the tandem catalysts with (a) H30, (b) H280, and (c) nH371 zeolites. Reaction conditions: 420 °C, 50 bar, 10 g_{cat} h mol_C^{-1}, $H_2/CO_x = 3$, $CO_2/CO_x = 0.5$.

effect of the particular reaction conditions in explaining the product distribution in the methanol/DME conversion is determined.

Fig. 10 displays the proposed reaction network for the direct production of hydrocarbons by the hydrogenation of CO_2/CO mixtures over tandem catalyst, based on previous results on the synthesis of oxygenates over ZnO–ZrO₂ catalyst [34], and those shown in previous sections. The first step considers the CO_2/CO hydrogenation into methanol/DME (with relevant formation of DME by the presence of an acid catalyst), and it also contemplates that this catalyst promotes the rWGS reaction and the undesired hydrogenation of CO_2/CO into methane [31]. Methane is also formed by the decomposition of the oxygenates (in particular from DME, which is less stable than methanol) [77]. The first steps of methanol/DME conversion into hydrocarbons are those corresponding to the dual-cycle mechanism, the extent of which is severely conditioned by the particular conditions of this process, in particular by the high partial pressure of H_2. Thus, the primary products with a C–C bond (C_2-C_4 olefins) are hydrogenated to form the corresponding paraffins and oligomerized to C_{5+} olefins, which will also be hydrogenated to the corresponding C_{5+} paraffins. In addition, the olefins will form naphthenes by cyclization reactions. The acidity of the zeolite used will play a relevant role in the extent of these reactions, shifting the equilibrium in the synthesis of oxygenates and promoting the formation of paraffins by hydrogen transfer reactions (as a complementary mechanism to the hydrogenation activated by the ZnO–ZrO₂ catalyst), and also the isomerization of these paraffins. In addition, the increase in acidity and density of acid sites will favor the extent of secondary reactions, highlighting for its importance in the production of C_{5+} hydrocarbons, its cracking to C_2-C_4 olefins and C_2-C_4 paraffins. Even if its importance is relatively small (it can be relevant at high values of time on stream), the formation of coke has been

considered in the scheme of Fig. 10, whose mechanism goes through the conversion of methanol/DME into hydrocarbons, by the condensation and the evolution of the aromatics towards condensed polyaromatic structures [78]. The high partial pressure of H_2 and the hydrogenating activity of the ZnO–ZrO₂ catalyst justify the negligible extent of the dehydrogenation of naphthenes to aromatics and consequently, the very limited deactivation of the catalyst by coke formation with all zeolites studied. Thus, by means of temperature programmed oxidation (TPO) analysis (TA Instruments TGA Q5000 thermobalance), it was determined that the content of coke deposited in catalysts ZZ/H280 and ZZ/nH371, in 6-hour runs, was less than 1 wt%. On the other hand, the coke content in ZZ/H30 and ZZ/ZnH30 catalysts was around 2 wt%, which is in line with the aforementioned effect of acidity.

The aforementioned results of hydrocarbons distribution are conditioned by the particular reaction conditions of the integrated process, which are different to the conventional conditions of the studies of methanol/DME conversion into hydrocarbons. Shi and Bhan [79] have established useful metrics to assess the effect of catalyst properties and reaction conditions on the conversion of methanol/DME into hydrocarbons. Given the interest of this approach, the metrics were calculated in the particular conditions under which the conversion of oxygenates takes place in this process. This way, the reduced olefins/paraffins (O/P) ratio, with values between 0.06 (with ZZ/nH371 catalyst) and 0.09 (with ZZ/H30 catalyst) is explained because the reaction conditions favor the hydrogenation of olefins, increasing the degree of product saturation. Similarly, the operating conditions affect the hydrogen transfer index (HTI), which represents the paraffin content with respect to the total hydrocarbons. Due to the high partial pressure and the hydrogenating capacity of ZnO–ZrO₂, the values of the HTI index are high, between 0.92 with ZZ/H30 catalyst and 0.94 with ZZ/nH371 catalyst.
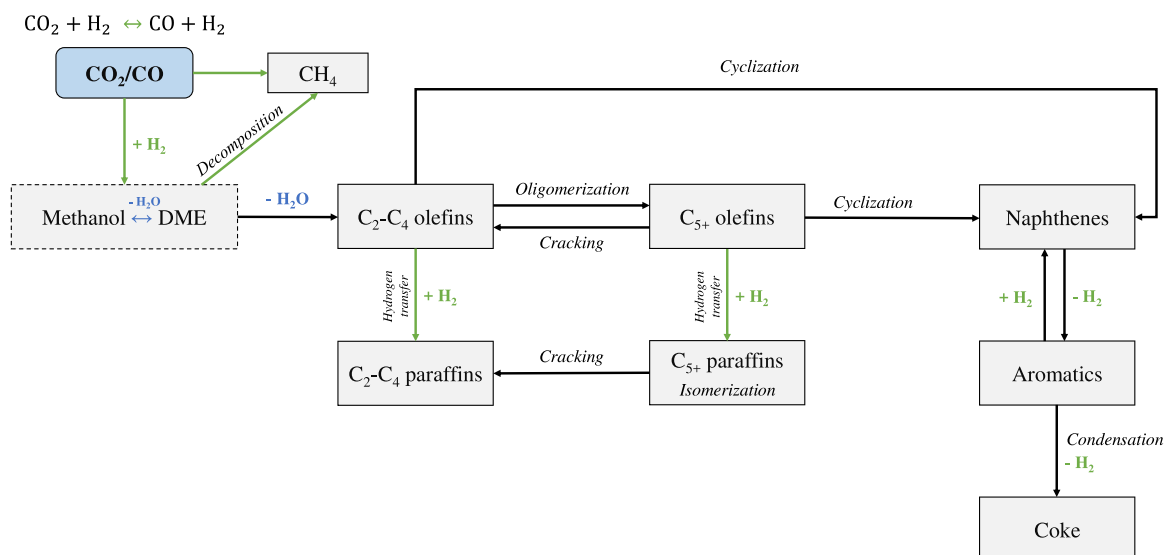
$$CO_2 + H_2 \leftrightarrow CO + H_2$$

Fig. 10. Proposed reaction network for the direct production of hydrocarbons by CO_2/CO mixture hydrogenation over the ZnO–ZrO$_2$/HZSM-5 catalysts.

The olefin/2-methylbutane ratio is proposed by the group of Bhan to assess the relative importance of the aromatics and olefins cycles in dual-cycle mechanism [80]. The value of this index were in the 0.8–2.4 range in the conversion of methanol over HZSM-5 zeolite at near atmospheric pressure and absence of H_2. However, the results of this index in the present work are very low, between 0.032 with ZZ/H30 catalyst and 0.048 with ZZ/nH371 catalyst, indicating a small relative extent of the aromatic cycle in the conditions (high partial pressure of H_2) of the integrated process.

4. Conclusions

The interest of the ZnO–ZrO$_2$/HZSM-5 tandem catalyst for the direct production of hydrocarbons by hydrogenation of a CO_2/CO mixture, and the importance of the role of the zeolite properties, and in particular of the acidity, in the hydrocarbon distribution was proved. The objective of a high production of the C$_{5+}$ fraction was achieved with a zeolite of low acidity (<100 $\mu mol_{NH_3} g_{cat}^{-1}$) as corresponds to a high SiO$_2$/Al$_2$O$_3$ ratio, and the results were further improved using nanosized particles. A yield and selectivity of C$_{5+}$ hydrocarbons of 19.6% and 78%, respectively, with a CO$_x$ (CO$_2$+CO) conversion of 25.1% was obtained with ZZ/nH371. The composition of this C$_{5+}$ fraction, with C$_5$ and C$_6$ paraffins (mainly isoparaffins) as major products (RON of 91) and absence of aromatics and heteroatoms, is particularly interesting for its incorporation into the refinery gasoline pool. A high acidity and the presence of strong acid sites in the zeolite is not suitable, because it favors the extent of secondary cracking reactions, with formation of C$_2$-C$_4$ hydrocarbons (mostly paraffins) and CH$_4$, appreciating also a negative synergy with the activity of the ZnO–ZrO$_2$ catalyst.

The synergy of the reaction steps catalyzed by the ZnO–ZrO$_2$ and HZSM-5 catalysts and the particular conditions of the integrated process (with a high H_2 partial pressure) justify the results, favoring the formation of mostly paraffins and minimizing the formation of aromatics.

The reaction network proposed for the process facilitates the understanding of the extent of the reaction steps of the methanol/DME conversion under the particular conditions of this process. Thus, the high partial pressure of H_2 conditions the extent of these steps and consequently the results (yield and selectivity). This different relative importance of the reaction stages, minimizing the formation of aromatics and coke, and favoring the formation of mostly paraffins, must be taken into account to interpret the evolution of the established dual-cycle mechanism under the conditions of this process. Thus, the

metrics established in conditions of the methanol/DME conversion in hydrocarbons (near atmospheric pressure and in the absence of H_2) are significantly modified.

CRediT authorship contribution statement

Onintze Parra: Writing – original draft, Investigation, Visualization, Formal analysis, Data curation, Conceptualization. **Ander Portillo:** Methodology, Investigation, Formal analysis, Data curation, Conceptualization. **Zuria Tabernilla:** Visualization, Investigation, Formal analysis, Data curation. **Andrés T. Aguayo:** Visualization, Supervision, Methodology, Data curation, Conceptualization. **Javier Ereña:** Supervision, Project administration, Funding acquisition. **Javier Bilbao:** Writing – original draft, Visualization, Supervision, Methodology, Data curation, Conceptualization. **Ainara Ateka:** Writing – original draft, Supervision, Project administration, Funding acquisition, Data curation, Conceptualization.

Declaration of competing interest

The authors declare that they have no known competing financial interests or personal relationships that could have appeared to influence the work reported in this paper.

Acknowledgments

Appendix A. Supplementary data

Supplementary material related to this article can be found online at https://doi.org/10.1016/j.renene.2024.121693.

References

[1] M.W. Jones, G.P. Peters, T. Gasser, R.M. Andrew, C. Schwingshackl, J. Gütschow, R.A. Houghton, P. Friedlingstein, J. Pongratz, C. Le Quéré, National contributions to climate change due to historical emissions of carbon dioxide, methane, and nitrous oxide since 1850, Sci. Data 10 (1) (2023) 155, http://dx.doi.org/10.1038/s41597-023-02041-1.

[2] T. Li, J. Long, W. Du, F. Qian, V. Mahalec, Three pathways towards elimination of CO_2 emissions from industrial plants that use hydrocarbon fuels, J. Clean. Prod. 391 (2023) 136159, http://dx.doi.org/10.1016/j.jclepro.2023.136159.

[3] A.D. Kamkeng, M. Wang, J. Hu, W. Du, F. Qian, Transformation technologies for CO_2 utilisation: Current status, challenges and future prospects, Chem. Eng. J. 409 (2021) 128138, http://dx.doi.org/10.1016/j.cej.2020.128138.

[4] A. Ateka, P. Rodriguez-Vega, J. Ereña, A.T. Aguayo, J. Bilbao, A review on the valorization of CO_2. Focusing on the thermodynamics and catalyst design studies of the direct synthesis of dimethyl ether, Fuel Process. Technol. 233 (2022) 107310, http://dx.doi.org/10.1016/j.fuproc.2022.107310.

[5] T.A. Atsbha, T. Yoon, P. Seongho, C.J. Lee, A review on the catalytic conversion of CO_2 using H_2 for synthesis of CO, methanol, and hydrocarbons, J. CO2 Util. 44 (2021) 101413, http://dx.doi.org/10.1016/j.jcou.2020.101413.

[6] R. Estevez, L. Aguado-Deblas, F.M. Bautista, F.J. López-Tenllado, A.A. Romero, D. Luna, A review on green hydrogen valorization by heterogeneous catalytic hydrogenation of captured CO_2 into value-added products, Catalysts 12 (12) (2022) 1555, http://dx.doi.org/10.3390/catal12121555.

[7] X. Jiang, X. Nie, X. Guo, C. Song, J.G. Chen, Recent advances in carbon dioxide hydrogenation to methanol via heterogeneous catalysis, Chem. Rev. 120 (15) (2020) 7984–8034, http://dx.doi.org/10.1021/acs.chemrev.9b00723.

[8] J. Niu, H. Liu, Y. Jin, B. Fan, W. Qi, J. Ran, Comprehensive review of Cu-based CO_2 hydrogenation to CH_3OH: Insights from experimental work and theoretical analysis, Int. J. Hydrog. Energy 47 (15) (2022) 9183–9200, http://dx.doi.org/10.1016/j.ijhydene.2022.01.021.

[9] L. Cui, C. Liu, B. Yao, P.P. Edwards, T. Xiao, F. Cao, A review of catalytic hydrogenation of carbon dioxide: From waste to hydrocarbons, Front. Chem. 10 (2022) http://dx.doi.org/10.3389/fchem.2022.1037997.

[10] A.T. To, M.A. Arellano-Treviño, C.P. Nash, D.A. Ruddy, Direct synthesis of branched hydrocarbons from CO_2 over composite catalysts in a single reactor, J. CO2 Util. 66 (2022) 102261, http://dx.doi.org/10.1016/j.jcou.2022.102261.

[11] A. Ramirez, A. Dutta Chowdhury, A. Dokania, P. Cnudde, M. Caglayan, I. Yarulina, E. Abou-Hamad, L. Gevers, S. Ould-Chikh, K. De Wispelaere, V. Van Speybroeck, J. Gascon, Effect of zeolite topology and reactor configuration on the direct conversion of CO_2 to light olefins and aromatics, ACS Catal. 9 (7) (2019) 6320–6334, http://dx.doi.org/10.1021/acscatal.9b01466.

[12] P. Lu, J. Liang, K. Wang, B. Liu, T. Atchimarungsri, Y. Wang, X. Zhang, J. Tian, Y. Jiang, Z. Liu, P. Reubroycharoen, T. Zhao, J. Zhang, X. Gao, Boosting liquid hydrocarbon synthesis from CO_2 hydrogenation via tailoring acid properties of HZSM-5 zeolite, Ind. Eng. Chem. Res. 61 (44) (2022) 16393–16401, http://dx.doi.org/10.1021/acs.iecr.2c03132.

[13] P. Sharma, J. Sebastian, S. Ghosh, D. Creaser, L. Olsson, Recent advances in hydrogenation of CO_2 into hydrocarbons via methanol intermediate over heterogeneous catalysts, Catal. Sci. Technol. 11 (5) (2021) 1665–1697, http://dx.doi.org/10.1039/d0cy01913e.

[14] A. Ateka, P. Pérez-Uriarte, M. Gamero, J. Ereña, A.T. Aguayo, J. Bilbao, A comparative thermodynamic study on the CO_2 conversion in the synthesis of methanol and of DME, Energy 120 (2017) 796–804, http://dx.doi.org/10.1016/j.energy.2016.11.129.

[15] T. Cordero-Lanzac, C. Martínez, A.T. Aguayo, P. Castaño, J. Bilbao, A. Corma, Activation of n-pentane while prolonging HZSM-5 catalyst lifetime during its combined reaction with methanol or dimethyl ether, Catal. Today 383 (2022) 320–329, http://dx.doi.org/10.1016/j.cattod.2020.09.015.

[16] N.J. Azhari, D. Erika, S. Mardiana, T. Ilmi, M.L. Gunawan, I.G. Makertihartha, G.T. Kadja, Methanol synthesis from CO_2: A mechanistic overview, Results Eng. 16 (2022) 100711, http://dx.doi.org/10.1016/j.rineng.2022.100711.

[17] M. Kauppinen, A. Posada-Borbón, H. Grönbeck, Methanol synthesis over PdIn, In_2O_3, and CuZn from first-principles microkinetics: Similarities and differences, J. Phys. Chem. C 126 (36) (2022) 15235–15246, http://dx.doi.org/10.1021/acs.jpcc.2c05715.

[18] M. Bjørgen, S. Svelle, F. Joensen, J. Nerlov, S. Kolboe, F. Bonino, L. Palumbo, S. Bordiga, U. Olsbye, Conversion of methanol to hydrocarbons over zeolite H-ZSM-5: On the origin of the olefinic species, J. Catal. 249 (2) (2007) 195–207, http://dx.doi.org/10.1016/j.jcat.2007.04.006.

[19] A. Portillo, O. Parra, J. Ereña, A. Aguayo, J. Bilbao, A. Ateka, Effect of water and methanol concentration in the feed on the deactivation of In_2O_3-ZrO_2/SAPO-34 catalyst in the conversion of CO_2/CO to olefins by hydrogenation, Fuel 346 (2023) 128298, http://dx.doi.org/10.1016/J.fuel.2023.128298.

[20] S.K. Saw, S. Datta, P.D. Chavan, P.K. Gupta, S. Kumari, G. Sahu, V. Chauhan, Significance and influence of various promoters on Cu-based catalyst for synthesizing methanol from syngas: a critical review, J. Chem. Technol. Biotechnol. 98 (5) (2023) 1083–1102, http://dx.doi.org/10.1002/jctb.7331.

[21] N. Yusuf, F. Almomani, Highly effective hydrogenation of CO_2 to methanol over $Cu/ZnO/Al_2O_3$ catalyst: A process economy & environmental aspects, Fuel 332 (2023) 126027, http://dx.doi.org/10.1016/j.fuel.2022.126027.

[22] X. Dong, S. Ma, P. Gao, The development of uncalcined Cu-based catalysts by liquid reduction method for CO_2 hydrogenation to methanol, Catal. Lett. (2022) http://dx.doi.org/10.1007/s10562-022-04093-1.

[23] W. Gao, L. Guo, Y. Cui, G. Yang, Y. He, C. Zeng, A. Taguchi, T. Abe, Q. Ma, Y. Yoneyama, N. Tsubaki, Selective Conversion of CO_2 into para-Xylene over a $ZnCr_2O_4$-ZSM-5 Catalyst, ChemSusChem 13 (24) (2020) 6541–6545, http://dx.doi.org/10.1002/cssc.202002305.

[24] A. Portillo, A. Ateka, J. Ereña, J. Bilbao, A. Aguayo, Role of Zr loading into In_2O_3 catalysts for the direct conversion of CO_2/CO mixtures into light olefins, J. Environ. Manag. 316 (2022) 115329, http://dx.doi.org/10.1016/j.jenvman.2022.115329.

[25] T. Cordero-Lanzac, A. Ramirez, M. Cruz-Fernandez, H.J. Zander, F. Joensen, S. Woolass, A. Meiswinkel, P. Styring, J. Gascon, U. Olsbye, A CO_2 valorization plant to produce light hydrocarbons: Kinetic model, process design and life cycle assessment, J. CO2 Util. 67 (2023) 102337, http://dx.doi.org/10.1016/j.jcou.2022.102337.

[26] W. Zhang, S. Wang, S. Guo, Z. Qin, M. Dong, W. Fan, J. Wang, GamCrOx/H-SAPO-34(F), a highly efficient bifunctional catalyst for the direct conversion of CO_2 into ethene and propene, Fuel 329 (2022) 125475, http://dx.doi.org/10.1016/j.fuel.2022.125475.

[27] P. Tian, Z. Zhan, J. Tian, K.B. Tan, M. Guo, Y. Han, T. Fu, J. Huang, Q. Li, Direct CO_2 hydrogenation to light olefins over $ZnZrO_x$ mixed with hierarchically hollow SAPO-34 with rice husk as green silicon source and template, Appl. Catal. B 315 (2022) 121572, http://dx.doi.org/10.1016/j.apcatb.2022.121572.

[28] L. Zhang, W. Gao, F. Wang, C. Wang, J. Liang, X. Guo, Y. He, G. Yang, N. Tsubaki, Highly selective synthesis of light aromatics from CO_2 by chromium-doped ZrO_2 aerogels in tandem with $HZSM-5@SiO_2$ catalyst, Appl. Catal. B 328 (2023) 122535, http://dx.doi.org/10.1016/j.apcatb.2023.122535.

[29] A. Portillo, A. Ateka, J. Ereña, A.T. Aguayo, J. Bilbao, Conditions for the joint conversion of CO_2 and syngas in the direct synthesis of light olefins using In_2O_3-ZrO_2/SAPO-34 catalyst, Ind. Eng. Chem. Res. 61 (29) (2022) 10365–10376, http://dx.doi.org/10.1021/acs.iecr.1c03556.

[30] P. Lu, X. Chang, W. Yu, Q. Hu, K.M. Ali, C. Xing, C. Du, Z. Yang, S. Chen, Synergistic effects of ZnO–ZrO_2@SAPO-34 core-shell catalyst in catalyzing CO_2 hydrogenation for the synthesis of light olefins, Renew. Energ. 209 (2023) 546–557, http://dx.doi.org/10.1016/j.renene.2023.03.111.

[31] O. Parra, A. Portillo, J. Ereña, A.T. Aguayo, J. Bilbao, A. Ateka, Boosting the activity in the direct conversion of CO_2/CO mixtures into gasoline using ZnO-ZrO_2 catalyst in tandem with HZSM-5 zeolite, Fuel Process. Technol. 245 (2023) 107745, http://dx.doi.org/10.1016/j.fuproc.2023.107745.

[32] S. Ghosh, L. Olsson, D. Creaser, Methanol mediated direct CO_2 hydrogenation to hydrocarbons: Experimental and kinetic modeling study, Chem. Eng. J. 435 (2022) 135090, http://dx.doi.org/10.1016/j.cej.2022.135090.

[33] C.T. Nimlos, C.P. Nash, D.P. Dupuis, A.T. To, A. Kumar, J.E. Hensley, D.A. Ruddy, Direct conversion of renewable CO2-rich syngas to high-octane hydrocarbons in a single reactor, ACS Catal. 12 (15) (2022) 9270–9280, http://dx.doi.org/10.1021/acscatal.2c02155.

[34] J. Ding, Z. Li, W. Xiong, Y. Zhang, A. Ye, W. Huang, Structural evolution and catalytic performance in CO_2 hydrogenation reaction of ZnO-ZrO_2 composite oxides, Appl. Surf. Sci. 587 (2022) http://dx.doi.org/10.1016/j.apsusc.2022.152884.

[35] J. Wang, G. Li, Z. Li, C. Tang, Z. Feng, H. An, H. Liu, T. Liu, C. Li, A highly selective and stable ZnO-ZrO_2 solid solution catalyst for CO_2 hydrogenation to methanol, Sci. Adv. 3 (10) (2017) http://dx.doi.org/10.1126/sciadv.1701290.

[36] P. Ticali, D. Salusso, R. Ahmad, C. Ahoba-Sam, A. Ramirez, G. Shterk, K.A. Lomachenko, E. Borfecchia, S. Morandi, L. Cavallo, J. Gascon, S. Bordiga, U. Olsbye, CO_2 hydrogenation to methanol and hydrocarbons over bifunctional Zn-doped ZrO_2/zeolite catalysts, Catal. Sci. Technol. 11 (4) (2021) 1249–1268, http://dx.doi.org/10.1039/d0cy01550d.

[37] T. Wang, C. Yang, P. Gao, S. Zhou, S. Li, H. Wang, Y. Sun, ZnZrOx integrated with chain-like nanocrystal HZSM-5 as efficient catalysts for aromatics synthesis from CO_2 hydrogenation, Appl. Catal. B 286 (2021) 119929, http://dx.doi.org/10.1016/j.apcatb.2021.119929.

[38] W. Li, G. Zhan, X. Liu, Y. Yue, K.B. Tan, J. Wang, J. Huang, Q. Li, Assembly of ZnZrOx and ZSM-5 on hierarchically porous bio-derived SiO_2 platform as bifunctional catalysts for CO_2 hydrogenation to aromatics, Appl. Catal. B 330 (2023) 122575, http://dx.doi.org/10.1016/j.apcatb.2023.122575.

[39] C.D. Chang, A.J. Silvestri, The conversion of methanol and other O-compounds to hydrocarbons over zeolite catalysts, J. Catal. 47 (2) (1977) 249–259, http://dx.doi.org/10.1016/0021-9517(77)90172-5.

[40] Z. Wan, G.K. Li, C. Wang, H. Yang, D. Zhang, Relating coke formation and characteristics to deactivation of ZSM-5 zeolite in methanol to gasoline conversion, Appl. Catal. A-Gen. 549 (2018) 141–151, http://dx.doi.org/10.1016/j.apcata.2017.09.035.

[41] R. Feng, B. Liu, P. Zhou, X. Yan, X. Hu, M. Zhou, Z. Yan, Influence of framework Al distribution in HZSM-5 channels on catalytic performance in the methanol to propylene reaction, Appl. Catal. A-Gen. 629 (2022) 118422, http://dx.doi.org/10.1016/j.apcata.2021.118422.

[42] P.L. Benito, A.G. Gayubo, A.T. Aguayo, M. Olazar, J. Bilbao, Effect of Si/Al ratio and of acidity of H-ZSM5 zeolites on the primary products of methanol to gasoline conversion, J. Chem. Technol. Biotechnol. 66 (2) (1996) 183–191, http://dx.doi.org/10.1002/(sici)1097-4660(199606)66:2<183::aid-jctb487>3.0.co;2-k.

[43] T. Cordero-Lanzac, A. Ateka, P. Pérez-Uriarte, P. Castaño, A.T. Aguayo, J. Bilbao, Insight into the deactivation and regeneration of HZSM-5 zeolite catalysts in the conversion of dimethyl ether to olefins, Ind. Eng. Chem. Res. 57 (41) (2018) 13689–13702, http://dx.doi.org/10.1021/acs.iecr.8b03308.

[44] J. Gao, H. Zhou, F. Zhang, K. Ji, P. Liu, Z. Liu, K. Zhang, Effect of preparation method on the catalytic performance of HZSM-5 zeolite catalysts in the MTH reaction, Materials 15 (2022) 2206, http://dx.doi.org/10.3390/ma15062206.

[45] Y. Zhang, Y. Qu, J. Wang, Effect of crystal size on the catalytic performance of HZSM-5 Zeolite in the methanol to aromatics reaction, Pet. Sci. Technol. 36 (12) (2018) 898–903, http://dx.doi.org/10.1080/10916466.2018.1451889.

[46] A. Xing, N. Zhang, D. Yuan, H. Liu, Y. Sang, P. Miao, Q. Sun, M. Luo, Relationship between acidity, defective sites, and diffusion properties of nanosheet ZSM-5 and its catalytic performance in the methanol to propylene reaction, Ind. Eng. Chem. Res. 58 (28) (2019) 12506–12515, http://dx.doi.org/10.1021/acs.iecr.9b00325.

[47] A. Zheng, Z. Zhao, S. Chang, Z. Huang, H. Wu, X. Wang, F. He, H. Li, Effect of crystal size of ZSM-5 on the aromatic yield and selectivity from catalytic fast pyrolysis of biomass, J. Mol. Catal. A Chem. 383–384 (2014) 23–30, http://dx.doi.org/10.1016/j.molcata.2013.11.005.

[48] Z. Wen, C. Wang, J. Wei, J. Sun, L. Guo, Q. Ge, H. Xu, Isoparaffin-rich gasoline synthesis from DME over Ni-modified HZSM-5, Catal. Sci. Technol. 6 (2016) 8089–8097, http://dx.doi.org/10.1039/c6cy01818a.

[49] X. Zhao, J. Li, P. Tian, L. Wang, X. Li, S. Lin, X. Guo, Z. Liu, Achieving a superlong lifetime in the zeolite-catalyzed MTO reaction under high pressure: Synergistic effect of hydrogen and water, ACS Catal. 9 (4) (2019) 3017–3025, http://dx.doi.org/10.1021/acscatal.8b04402.

[50] T. Shoinkhorova, T. Cordero-Lanzac, A. Ramirez, S.H. Chung, A. Dokania, J. Ruiz-Martinez, J. Gascon, Highly selective and stable production of aromatics via high-pressure methanol conversion, ACS Catal. 11 (6) (2021) 3602–3613, http://dx.doi.org/10.1021/acscatal.0c05133.

[51] L.N. Vosmerikova, Z.M. Matieva, Y.M. Snatenkova, N.V. Kolesnichenko, V.I. Zaikovskii, A.V. Vosmerikov, Conversion of dimethyl ether to liquid hydrocarbons over Zn-isomorphously substituted HZSM-5, Fuel 320 (2022) 123959, http://dx.doi.org/10.1016/j.fuel.2022.123959.

[52] X. Su, K. Zhang, Y. Snatenkova, Z. Matieva, X. Bai, N. Kolesnichenko, W. Wu, High-efficiency nano [Zn,Al]ZSM-5 bifunctional catalysts for dimethyl ether conversion to isoparaffin-rich gasoline, Fuel Process. Technol. 198 (2020) 106242, http://dx.doi.org/10.1016/g.fuproc.2019.106242.

[53] R. Khare, D. Millar, A. Bhan, A mechanistic basis for the effects of crystallite size on light olefin selectivity in methanol-to-hydrocarbons conversion on MFI, J. Catal. 321 (2015) 23–31, http://dx.doi.org/10.1016/j.jcat.2014.10.016.

[54] R. Khare, Z. Liu, Y. Han, A. Bhan, A mechanistic basis for the effect of aluminum content on ethene selectivity in methanol-to-hydrocarbons conversion on HZSM-5, J. Catal. 348 (2017) 300–305, http://dx.doi.org/10.1016/j.jcat.2017.02.022.

[55] B. Pawelec, R. Mariscal, R.M. Navarro, J.M. Campos-Martin, J.L. Fierro, Simultaneous 1-pentene hydroisomerisation and thiophene hydrodesulphurisation over sulphided Ni/FAU and Ni/ZSM-5 catalysts, Appl. Catal. A-Gen. 262 (2) (2004) 155–166, http://dx.doi.org/10.1016/j.apcata.2003.11.037.

[56] P. Pérez-Uriarte, M. Gamero, A. Ateka, M. Díaz, A.T. Aguayo, J. Bilbao, Effect of the acidity of HZSM-5 zeolite and the binder in the DME transformation to olefins, Ind. Eng. Chem. Res. 55 (2016) 1513–1521, http://dx.doi.org/10.1021/acs.iecr.5b04477.

[57] M. Lefrancois, G. Malbois, The nature of the acidic sites on mordenite. Characterization of adsorbed pyridine and water by infrared study, J. Catalysis 20 (3) (1971) 350–358, http://dx.doi.org/10.1016/0021-9517(71)90097-2.

[58] J.W. Ward, The nature of active sites on zeolites. I. The decationated Y zeolite, J. Catalysis 9 (3) (1967) 225–236, http://dx.doi.org/10.1016/0021-9517(67)90248-5.

[59] Z. Wan, W. Wu, G.K. Li, C. Wang, H. Yang, D. Zhang, Effect of SiO₂/Al₂O₃ ratio on the performance of nanocrystal ZSM-5 zeolite catalysts in methanol to gasoline conversion, Appl. Catal. A-Gen. 523 (2016) 312–320, http://dx.doi.org/10.1016/j.apcata.2016.05.032.

[60] N. Viswanadham, R. Kamble, M. Singh, M. Kumar, G. Murali Dhar, Catalytic properties of nano-sized ZSM-5 aggregates, Catal. Today 141 (1–2) (2009) 182–186, http://dx.doi.org/10.1016/j.cattod.2008.03.026.

[61] Z. Han, F. Zhou, J. Zhao, Y. Liu, H. Ma, G. Wu, Synthesis of hierarchical GaZSM-5 zeolites by a post-treatment method and their catalytic conversion of methanol to olefins, Microp. Mesop. Mat. 302 (2020) 110194, http://dx.doi.org/10.1016/j.micromeso.2020.110194.

[62] Z. Song, A. Takahashi, I. Nakamura, T. Fujitani, Phosphorus-modified ZSM-5 for conversion of ethanol to propylene, Appl. Catal. A-Gen. 384 (2010) 201–205, http://dx.doi.org/10.1016/j.apcata.2010.06.035.

[63] M. Fattahi, R.M. Behbahani, T. Hamoule, Synthesis promotion and product distribution for HZSM-5 and modified Zn/HZSM-5 catalysts for MTG process, Fuel 181 (2016) 248–258, http://dx.doi.org/10.1016/j.fuel.2016.04.120.

[64] I. Pinilla-Herrero, E. Borfecchia, T. Cordero-Lanzac, U.V. Mentzel, F. Joensen, K.A. Lomachenko, S. Bordiga, U. Olsbye, P. Beato, S. Svelle, Finding the active species: The conversion of methanol to aromatics over Zn-ZSM-5/alumina shaped catalysts, J. Catal. 394 (2021) 416–428, http://dx.doi.org/10.1016/j.jcat.2020.10.024.

[65] R. Jin, K. Ma, Z. Chen, Z. Tang, H. Hu, J. Wang, Z. Zhang, C. Dai, X. Ma, Effect of CO₂ on the catalytic performance of Zn/ZSM-5 towards the conversion of methanol to aromatics, Fuel 332 (2023) 126247, http://dx.doi.org/10.1016/j.fuel.2022.126247.

[66] Y. Gao, B. Zheng, G. Wu, F. Ma, C. Liu, Effect of the Si/Al ratio on the performance of hierarchical ZSM-5 zeolites for methanol aromatization, RSC Adv. 6 (87) (2016) 83581–83588, http://dx.doi.org/10.1039/c6ra17084f.

[67] A. Portillo, A. Ateka, J. Ereña, J. Bilbao, A. Aguayo, Alternative acid catalysts for the stable and selective direct conversion of co₂/CO mixtures into light olefins, Fuel Process. Technol. 238 (2022) 107513, http://dx.doi.org/10.1016/j.fuproc.2022.107513.

[68] E. Kianfar, S. Hajimirzaee, S. Mousavian, A.S. Mehr, Zeolite-based catalysts for methanol to gasoline process: A review, Microchem. J. 156 (2020) 104822, http://dx.doi.org/10.1016/j.microc.2020.104822.

[69] G. Bonura, C. Cannilla, L. Frusteri, E. Catizzone, S. Todaro, M. Migliori, G. Giordano, F. Frusteri, Interaction effects between CuO-ZnO-ZrO₂ methanol phase and zeolite surface affecting stability of hybrid systems during one-step CO₂ hydrogenation to DME, Catal. Today 345 (2020) 175–182, http://dx.doi.org/10.1016/j.cattod.2019.08.014.

[70] A. García-Trenco, A. Vidal-Moya, A. Martínez, Study of the interaction between components in hybrid CuZnAl/HZSM-5 catalysts and its impact in the syngas-to-DME reaction, Catal. Today 179 (2012) 43–51, http://dx.doi.org/10.1016/j.cattod.2011.06.034.

[71] A. García-Trenco, A. Martínez, Direct synthesis of DME from syngas on hybrid cuZnAl/ZSM-5 catalysts: New insights into the role of zeolite acidity, Appl. Catal. A-Gen. 411–412 (2012) 170–179, http://dx.doi.org/10.1016/j.apcata.2011.10.036.

[72] E.A. Redekop, T. Cordero-Lanzac, D. Salusso, A. Pokle, S. Oien-Odegaard, M.F. Sunding, S. Diplas, C. Negri, E. Borfecchia, S. Bordiga, U. Olsbye, Zn redistribution and volatility in ZnZrOx catalysts for CO2 hydrogenation, Chem. Mater. 35 (24) (2023) 10434–10445, http://dx.doi.org/10.1021/acs.chemmater.3c01632.

[73] M. Yamamura, K. Chaki, T. Wakatsuki, H. Okado, K. Fujimoto, Synthesis of ZSM-5 zeolite with small crystal size and its catalytic performance for ethylene oligomerization, Zeolites 14 (1994) 643–649, http://dx.doi.org/10.1016/0144-2449(94)90121-X.

[74] S. Ilias, A. Bhan, Mechanism of the catalytic conversion of methanol to hydrocarbons, ACS Catal. 3 (2013) 18–31, http://dx.doi.org/10.1021/cs3006583.

[75] J.R. Esquius, H. Bahruji, M. Bowker, G.J. Hutchings, Identification of C₂-C₅ products from CO₂ hydrogenation over PdZn/TiO₂-ZSM-5 hybrid catalysts, Faraday Discuss. 230 (2021) 52–67, http://dx.doi.org/10.1039/d0fd00135j.

[76] P. Anderson, J. Sharkey, R. Walsh, Calculation of research octane number of motor gasolines from chromatographic data and a new approach to motor gasoline quality control, J. Inst. Pet. 59 (1972) 83.

[77] P. Pérez-Uriarte, A. Ateka, M. Gamero, A.T. Aguayo, J. Bilbao, Effect of the operating conditions in the transformation of DME to olefins over a HZSM-5 zeolite catalyst, Ind. Eng. Chem. Res. 55 (2016) 6569–6578, http://dx.doi.org/10.1021/acs.iecr.6b00627.

[78] M. Ibáñez, P. Pérez-Uriarte, M. Sánchez-Contador, T. Cordero-Lanzac, A.T. Aguayo, J. Bilbao, P. Castaño, Nature and location of carbonaceous species in a composite HZSM-5 zeolite catalyst during the conversion of dimethyl ether into light olefins, Catalysts 7 (2017) 254, http://dx.doi.org/10.3390/catal7090254.

[79] Z. Shi, A. Bhan, Metrics of performance relevant in methanol-to-hydrocarbons catalysis, J. Catal. 421 (2023) 198–209, http://dx.doi.org/10.1016/j.jcat.2023.03.022.

[80] S. Ilias, R. Khare, A. Malek, A. Bhan, A descriptor for the relative propagation of the aromatic- and olefin-based cycles in methanol-to-hydrocarbons conversion on HZSM-5, J. Catal. 303 (2013) 135–140, http://dx.doi.org/10.1016/j.jcat.2013.03.021.